

*Technical Report No. 32-927*

*Analysis of the Interaction of the Surveyor Radar  
Altimeter Doppler Velocity Sensor System and  
Vernier Thrust Chamber Plumes*

*A. J. Kelly*

GPO PRICE \$ \_\_\_\_\_  
CFSTI PRICE(S) \$ \_\_\_\_\_  
Hard copy (HC) \$11.00  
Microfiche (MF) 150

ff 653 July 65

FACILITY FORM 602

N66 26869	
(ACCESSION NUMBER)	(THRU)
22	1
(PAGES)	(CODE)
CR-75271	07
(NASA CR OR TMX OR AD NUMBER)	(CATEGORY)

JET PROPULSION LABORATORY  
CALIFORNIA INSTITUTE OF TECHNOLOGY  
PASADENA, CALIFORNIA

April 15, 1966

NATIONAL AERONAUTICS AND SPACE ADMINISTRATION

*Technical Report No. 32-927*

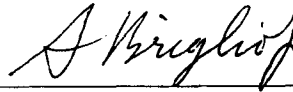
*Analysis of the Interaction of the Surveyor Radar  
Altimeter Doppler Velocity Sensor System and  
Vernier Thrust Chamber Plumes*

*A. J. Kelly*



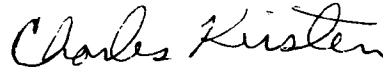
---

D. R. Bartz, Manager  
Research and Advanced Concepts



---

A. Briglio, Jr., Manager  
Spacecraft System Propulsion



---

C. C. Kirsten, Manager  
Spacecraft System Telecommunications

JET PROPULSION LABORATORY  
CALIFORNIA INSTITUTE OF TECHNOLOGY  
PASADENA, CALIFORNIA

April 15, 1966

Copyright © 1966  
Jet Propulsion Laboratory  
California Institute of Technology  
Prepared Under Contract No. NAS 7-100  
National Aeronautics & Space Administration

## CONTENTS

<b>I. Introduction</b> . . . . .	1
<b>II. Spacecraft Geometry</b> . . . . .	2
<b>III. Vernier Thrust Chamber No. 1 Plume, Doppler Beam No. 2 Geometry</b> . . . . .	4
<b>IV. Antenna Beam Geometry</b> . . . . .	5
<b>V. Plume Geometry</b> . . . . .	5
A. Gas Density . . . . .	5
B. Electron Density, $N_e$ . . . . .	6
C. Electron Collision Frequency, $\nu_e$ . . . . .	7
<b>VI. Beam-Plume Interaction</b> . . . . .	9
A. Relative Propagation Constant $K^*$ . . . . .	9
B. Applicability of the Phase Integral (WKBJ) Method . . . . .	10
C. Phase Shift . . . . .	10
D. Attenuation . . . . .	12
E. Reflections from the Plume . . . . .	13
F. Bending of the Beam . . . . .	13
<b>VII. Summary and Conclusions</b> . . . . .	15
A. Phase Shift . . . . .	15
B. Attenuation . . . . .	15
C. Reflection . . . . .	15
D. Beam Bending and Displacement . . . . .	15
<b>References</b> . . . . .	16

## TABLES

<b>1. Two-way phase shifts</b> . . . . .	11
<b>2. Change in two-way phase shift from normal</b> . . . . .	11
<b>3. Two-way signal attenuation</b> . . . . .	12

## FIGURES

<b>1. Plan view Surveyor</b> . . . . .	2
<b>2. RADVS beam orientation</b> . . . . .	3
<b>3. Vernier thrust chamber No. 1, doppler beam No. 2 geometry</b> . . . . .	4
<b>4. Plume, RADVS beam geometry</b> . . . . .	6
<b>5. <math>N_e/N_p</math> vs <math>\eta/\lambda_0</math></b> . . . . .	8

**ABSTRACT**

26869

This Report summarizes the analyses of the interaction of the *Surveyor* radar altimeter doppler velocity sensor (RADVS) system and vernier thrust chamber plumes. The investigation was occasioned by a study task initiated by JPL.

In keeping with guidelines of the study task outlines, this analysis was specifically conducted to provide conservative estimates of the vernier plume, RADVS-system interactions effects. In all instances, operating conditions were assumed which, while consistent with *Surveyor* system specifications, would exaggerate the RADVS-plume interaction. For example, the vernier propellant specifications permit a maximum total impurity concentration of 500 ppm. Actually, the propellant purity level is known, from test, to be at least an order of magnitude less than the specifications. However, for the purpose of this investigation, the propellant was assumed to have 500 ppm of sodium as an impurity. As with all other assumptions made during the course of analysis, this assumption permitted an upper bound to be placed on the interaction of the vernier plumes and the RADVS system. As a consequence, no attempt was made to provide a detailed assessment of the most probable level of RADVS-plume interaction to be expected under nominal *Surveyor* operating conditions.

The maximum calculated two-way attenuation and reflection level are both well below the levels at which the performance of the RADVS system would be significantly influenced. However, the nonstatic two-way phase-shift was found to be in excess of the level above which the operation of the RADVS system would be affected.

## I. INTRODUCTION

The *Surveyor* spacecraft has been expressly designed to permit the controlled deposition of a scientific and/or engineering payload on the lunar surface. This feat is to be accomplished by means of a controlled retro-rocket descent, from an Earth transfer trajectory, to within closely prescribed distances from the Moon.

Basically, the retro sequence conducted in the vicinity of the Moon can be divided into three distinct phases (Ref. 1). During the first phase, a radio altimeter located in the nozzle of the main solid retro-rocket provides an altitude ( $\sim 100$  km) marker signal which, when processed by the control circuitry of the spacecraft, initiates the main retro-rocket sequence. During retro burn, the three bipropellant vernier thrust chambers, used also for mid-course trajectory corrections, provide attitude control. Upon completion of the main retro-rocket burn, the spacecraft is within  $\sim 12$  km of the lunar surface, and its velocity has been reduced from  $\sim 2700$  m/sec to  $\sim 100$  m/sec. Twelve seconds after completion of the main retro burn, the solid propellant engine is ejected. At this point the spacecraft is  $\sim 8$  km from the surface and descending at a relative velocity of  $\sim 110$  m/sec. The initial phase of the landing maneuver is then complete.

The spacecraft is then at a sufficiently low altitude, relative to the surface of the Moon, that meaningful signals can be received by the doppler antennas and the

radio altimeter. The data from these antennas, which form a part of the radar altimeter and doppler velocity sensor (RADVS) system, are used to control the rate of descent and the attitude of the spacecraft by means of throttling of three vernier engines. Pitch and yaw are controlled by differential throttling of the verniers, while roll control (about the vertical, z-axis, of the spacecraft) is maintained by gimbaling (hinging) one of the vernier thrust chambers (vernier thrust chamber No. 1). The vernier engines operate continuously throughout the descent phase until an altitude of  $\sim 4$  m from the lunar surface is reached. At this point, if the flight control electronics have functioned as planned, the remaining velocity components, relative to the surface, will be less than  $\sim 2$  m/sec and the vernier engine thrusting is terminated.

During the third, and last, phase of the descent the spacecraft free-falls to the surface, the impact being absorbed by the structure of the bus.

Early in the *Surveyor* program, a study was conducted to determine whether, during the second phase of the landing sequence, the RADVS system would suffer a degradation in performance because of the free electrons present in the vernier exhaust plumes, through which the doppler velocity and radio-altimeter beams propagate. The analysis conducted by P. Molmud (Ref. 2) of STL

indicated that there would be no appreciable effect of the exhaust plumes on the RADVS system, for a similar spacecraft system.

This study is a reevaluation of the degree of interaction to be anticipated between the RADVS and the vernier

exhaust plumes. More recent data than were available to Molmud concerning the physical characteristics of the spacecraft have been used. In addition, a more careful evaluation of the anticipated back-scatter and the effects of throttling and gimbaling of the vernier engines has been included.

## II. SPACECRAFT GEOMETRY

As seen in the plan view of Fig. 1, the two RADVS antennas and the three vernier thrust chambers are arranged

on a circle that is roughly 1.9 m in diam. The exit plane of the vernier engines exhaust nozzles describe a plane

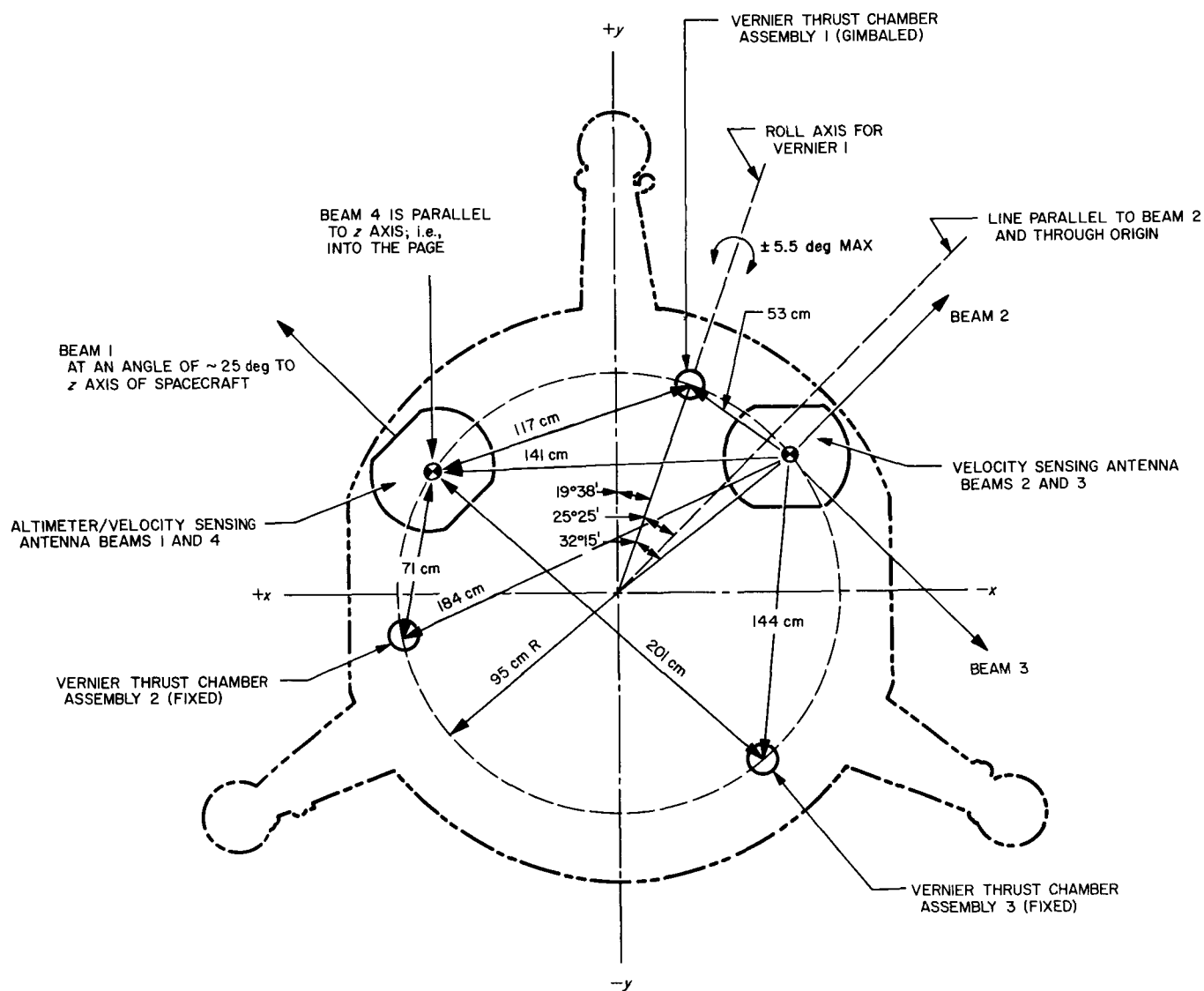


Fig. 1. Plan view Surveyor

which, to within narrow limits, passes through the center of the RADVS antenna apertures. The plan view depicts the directions in which the various doppler and radio altimeter beams propagate. A clearer picture of the geometry of these beams with reference to the spacecraft is presented in Fig. 2. All of the doppler beams lie, approximately, in a cone (half angle of 25 deg) with respect to the vertical spacecraft axis ( $z$  axis).

Consideration of these diagrams leads one to conclude that the most severe beam-plume interaction would occur between doppler beam No. 2 and the plume from vernier thrust chamber No. 1. This conclusion is based on the fact that the half of the antenna generating beam No. 2 and

the vernier thrust chamber No. 1 are in closer proximity than any other combination of antenna and thrust chamber and, moreover, vernier thrust chamber No. 1 is gimballed to provide spacecraft roll control. This gimbaling would, in effect, permit the plume to intersect more or less of the beam—depending on hinge position—therefore, changing the electron density environment through which the beam propagates in a variable manner over and above that which can be expected solely from the effects of throttling. Therefore, since the interaction of vernier thrust chamber No. 1 plume and the doppler beam No. 2 is the most severe, both statically (no throttling, no gimbaling) and dynamically (throttling and gimbaling of the thrust chamber), the study will be restricted to this case to the exclusion of all others.

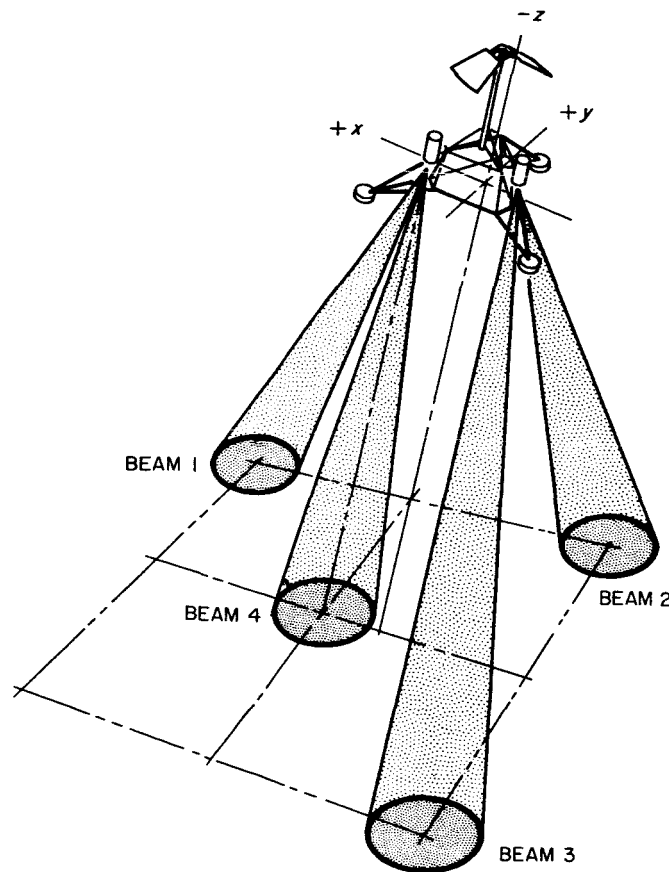


Fig. 2. RADVS beam orientation



### III. VERNIER THRUST CHAMBER NO. 1 PLUME, DOPPLER BEAM NO. 2 GEOMETRY

Figure 3 presents a diagram of the geometric relationships that exist between the center line of the plume generated by vernier thrust chamber No. 1 and the beam pattern produced by doppler antenna No. 2. From scale drawings of the spacecraft, the inter-axis spacing of vernier thrust chamber No. 1 and doppler antenna No. 2,  $a = 42$  cm. The vernier thrust chamber gimbals in a plane that intersects the plane formed by lines parallel to the  $z$  axis (drawn through the thrust chamber and antenna), at an angle  $\beta = 12.7$  deg. The gimbal angle  $\gamma$  can vary over the range of  $\pm 5\frac{1}{2}$  deg. For this analysis, only two

cases will be considered; the ungimbaled case where the thrust axis is vertical and  $\gamma = 0$ , and the case where thrust chamber No. 1 is gimbaled the maximum amount ( $5\frac{1}{2}$  deg) in the direction toward doppler beam No. 2. We shall denote distances along the plume axis (as measured from the thrust chamber exit plane) as  $\xi$  and distances measured from the antenna aperture plane along the beam axis as  $\eta$ . The first requirement is to determine the distance of closest approach ( $R$ ) of a given beam ray to an arbitrary point  $\xi$  on the plume axis by considering the geometry of the antenna beam.

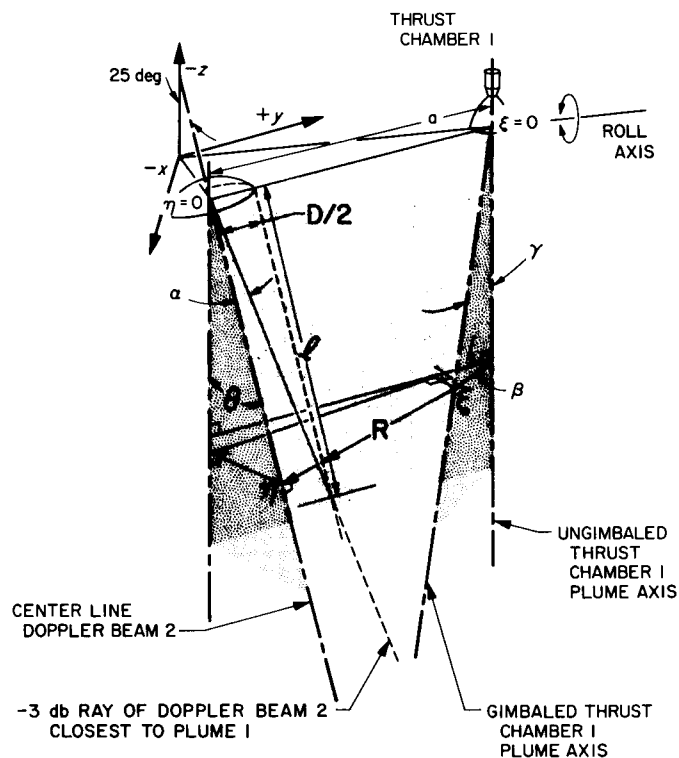


Fig. 3. Vernier thrust chamber No. 1, doppler beam No. 2 geometry

## IV. ANTENNA BEAM GEOMETRY

Two elliptical antennas, which are split so as to generate two separate and distinct beams for a total of four, comprise the antenna subsystem of the RADVS. The individual beams emanating from one half the RADVS antennas can be considered as being produced by an antenna having dimensions of  $\sim 25 \times 38$  cm. Using the average of these dimensions to characterize the antenna aperture dimensions, i.e.,  $D = 32$  cm, the calculated Rayleigh range  $l = D^2/2\lambda_0$ , for a frequency of 13.3 GHz ( $\lambda_0 = 2.25$  cm), is  $\sim 2.3$  m. This implies that the beam will be approximately collimated for  $\eta \leq 2.3$  m and then diverge at an angle  $\alpha$ , where  $\tan \alpha = \lambda_0/D$ , or  $\alpha = 4$  deg for  $\eta \geq 2.3$  m. Two beam rays are of particular interest,

the center ray representative of maximum beam power and the  $-3$ -db (half power) ray closest to the plume. The  $-3$ -db ray will be assumed to be emanating from the edge of the antenna, i.e., at a distance of  $D/2$  from the central (maximum power) ray. The  $-3$ -db ray is, in the Rayleigh near field region  $\eta \leq l$ , taken as parallel to the center ray and to lie on the surface of a cone of half-angle  $\alpha = 4$  deg for  $\eta \geq l$ , i.e., outside the Rayleigh near field zone. As will be subsequently demonstrated, a preponderant portion of the beam-plume interaction will occur in the near field region of the antenna, the fact that the assumed  $-3$ -db ray diverges for  $\eta \geq l$  is of relatively little importance, but is included for completeness.

## V. PLUME GEOMETRY

### A. Gas Density

It will be assumed that there is no interaction of beam No. 2 with other than electrons present in the plume from vernier thrust chamber No. 1. This assumption is deemed justified on the basis of the thrust-chamber spacing and the overall geometry of the plume. The plume geometry assumed for this program is that calculated<sup>1</sup> to exist for a conical (15-deg half-cone angle) nozzle exhausting into a vacuum, a gas with a ratio of specific heats  $C_p/C_v = 1.313$ . This ratio of specific heat is equivalent to what one would expect for the propellants used, i.e., nitrogen tetroxide (with 10% nitric oxide) and monomethylhydrazine monohydrate. While the actual vernier thrust chambers do have contoured nozzles, the error introduced into the calculation of the electron density profiles in the plume by the assumption of a 15-deg half-angle cone nozzle is considered to be insignificant.

In Fig. 4 are shown the Mach number profiles for the assumed conical nozzle, plotted in terms of dimensionless radial and longitudinal coordinates, i.e., coordinates normalized in terms of the thrust chamber exhaust plane

radius ( $R_e = 6.5$  cm). Also shown in the figure are the beam rays calculated for the four cases of interest, i.e., two gimbal positions of vernier thrust chamber No. 1 ( $\gamma = 0$  and  $5\frac{1}{2}$ -deg) and for each of the two beam rays of interest (central and  $-3$ -db ray closest to the plume). It should be noted that even though the rays have been assumed straight (this will be substantiated later) they appear curved in the figure. This is because the beam rays and the center line of the plume are askew, the radial distance  $R$  between the two being a non-linear function of the plume coordinate  $\xi$ .

The isentropic perfect gas relation

$$\rho_{\text{local}} = \rho_{\text{exit}} \left( \frac{1 + \frac{k-1}{2} M_{\text{exit}}^2}{1 + \frac{k-1}{2} M_{\text{local}}^2} \right)^{\frac{1}{k-1}}, \quad k = \frac{C_p}{C_v}$$

can now be used to evaluate the local gas density  $\rho$  as a function of the known Mach number  $M$  contours and the nozzle exit conditions. The following nozzle exit conditions are those anticipated to exist for the maximum thrust (47 kgf) condition

$$\rho_{\text{exit}} = 4.04 \times \frac{10^{-6} \text{ g}}{\text{cm}^3},$$

<sup>1</sup>McDermitt, C. Eugene, to Briglio, Jr., A., "Impingement Heating Rate Estimates of the Current RMD Exhaust Plume in the Vicinity of the Crushable Blocks and Altitude Marking Radar," Private Communication, Jet Propulsion Laboratory, Pasadena, Calif., 16 Sept. 1965.

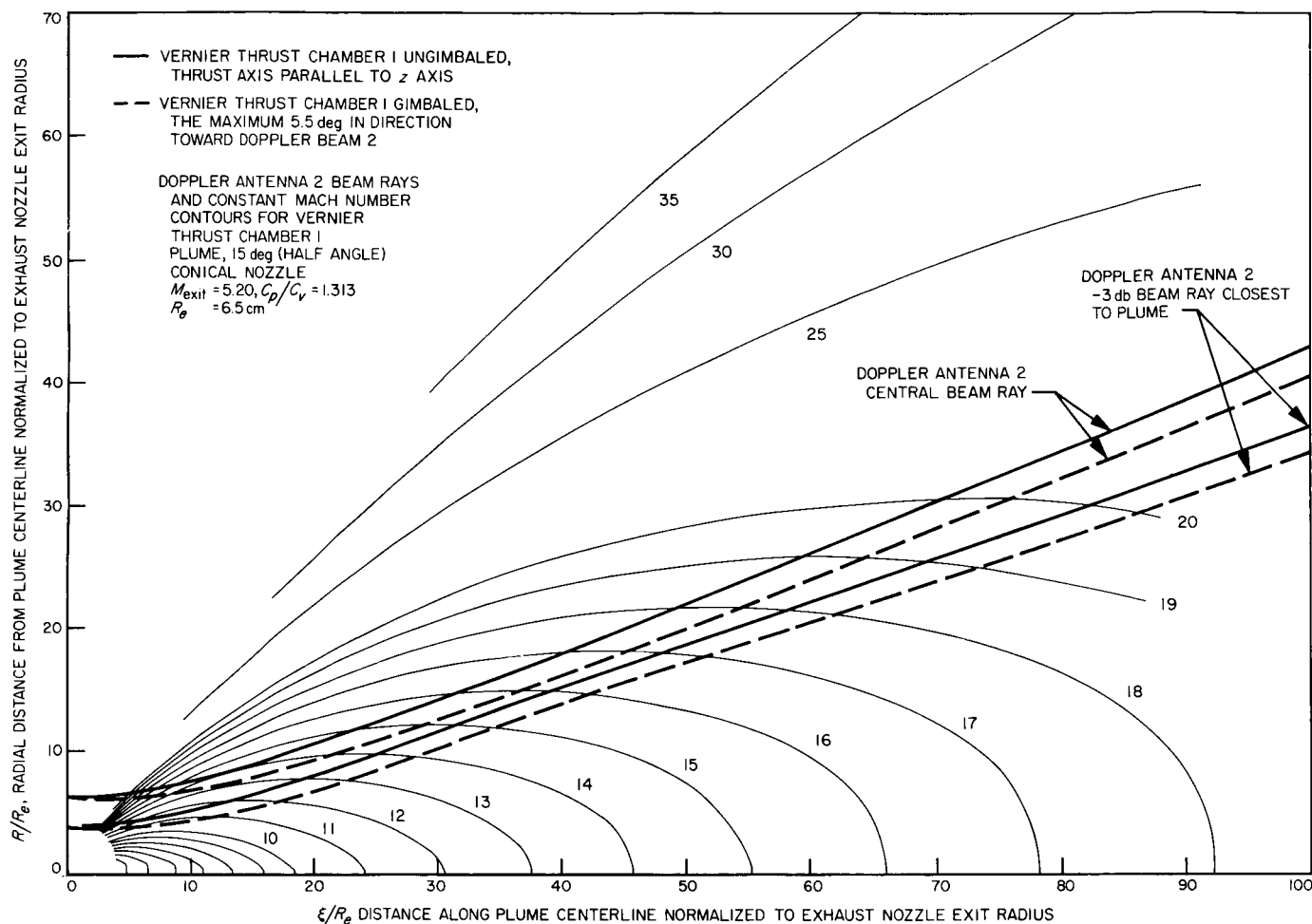


Fig. 4. Plume, RADVS beam geometry

( $N_a = 1.07 \times 10^{17} \text{ cm}^{-3}$  for  $M_{\text{exit}} = 22.77$ ), where  $N_a$  is the heavy particle density and  $M$  is the average molecular weight,

$$M_{\text{exit}} = 5.20, \quad k = \frac{C_p}{C_v} = 1.313$$

$$T_{\text{exit}} = 840^\circ\text{K}$$

The nominal expansion area ratio for this thrust chamber is 86:1.

### B. Electron Density $N_e$

To evaluate properly the electron density level present in the plume, it is necessary to consider the ionization processes associated with combustion. This, in turn, requires a knowledge of the level of low ionization level

impurities (alkali metals, etc.) present in the combustion gases. There are two sources of possible contamination, the propellants per se, and the material ablated from the chamber, throat, and nozzle liners. The JPL propellant specifications GMO-50427-MAT-A and GMO-50428-MAT-A require that there should be less than 500 ppm total impurities present in any batch of propellant specified for use. No information is currently available concerning the level of contamination caused by impurities present in the propulsion flow system which could be absorbed by the propellants during extended periods of storage. This source of contamination is thought to be small, i.e., less than 10 ppm. Actual analysis of samples of propellant indicate that extraneous impurities are less than 10 ppm, i.e., well below specification. The Rokide Z and silicon carbide coatings on the internal surfaces of the thrust chamber will erode slightly during operation. At most, it is estimated that  $\sim 6$  g of material will be ablated. The total propellant flowing through the system

is  $\sim 84$  kg. Therefore, ablation could contribute, on the average, a maximum of 60 ppm of contamination.

To cover all possible contingencies, it will be assumed that there are 500 ppm of contamination present in the exhaust gases. Moreover, to exaggerate the effect of this contamination, it will be taken to be comprised solely of sodium. These assumptions are quite conservative, insofar as the alkali metal content in the propellant is most probably on the order of 10 ppm or less. Consequently, the electron density, since it arises almost exclusively from ionization of the alkali metals present in the chamber gases, will be overestimated by at least an order of magnitude.

The chamber conditions used in the evaluation of the ionization level were:  $P_c = 17$  atm,  $N_a = 4.2 \times 10^{19} \text{ cm}^{-3}$ ,  $T_c = 2950^\circ\text{K}$ , gas composition = combustion products having an ionization potential of  $\sim 11$  ev plus 500 ppm of sodium (ionization potential 5.1 ev).

Application of the Saha equation for this two-species gas showed that only a negligibly small portion of the ionization level was due to the combustion products gas, the indicated ratio of electron to atom density

$$\frac{N_e}{N_a} \equiv c \simeq 2 \times 10^{-6}$$

arising from ionization of the sodium.

The ionization level calculated on the basis of chamber conditions was  $\sim 3 \times 10^{-6}$  and on the basis of throat conditions,  $\sim 0.7 \times 10^{-6}$ . It is anticipated that equilibrium conditions would prevail up to the throat and that the flow would be frozen downstream of this station. Accordingly, the ionization level was taken to be  $\sim 2 \times 10^{-6}$ . For comparison, if the flow were assumed to be in equilibrium through the nozzle and to be frozen in the plume the ionization level would be completely negligible, i.e., less than  $10^{-10}$ .

A series of tests have been conducted by W. Balwanz of the Naval Research Laboratories<sup>2</sup> (NRL) to determine exit plane electron densities of 23 kgf thrust chambers on alkali metal seeded *Surveyor* vernier thrust chamber propellants. The X-band focused microwave probe used in these tests indicated that, with sodium concentrations of

approximately 200 ppm (there were no tests at the 500 ppm level assumed in this study) and chamber conditions comparable to those encountered in the *Surveyor* vernier system, the electron density was, to within experimental error (a factor of  $\sim 2$ ), equal to that calculated for the exhaust plane of the vernier thrust chambers using the above assumptions.

It should be noted that the electron density is dependent upon the square root of the sodium concentration and that the thrust chambers tested had a somewhat smaller expansion area ratio than those used on *Surveyor*. Nevertheless, the agreement between the test results and the above calculations is exceptional and validates the assumptions used.

The assumption of a fixed ionization level, frozen at the averaged chamber-throat conditions, exaggerates the electron density level and is, therefore, conservative. This assumption permits one to relate the electron density level  $N_e$  very simply to the heavy particle density  $N_a$ , viz.  $N_e = c N_a$ . For the ensuing calculations, it is convenient to normalize the electron density to the electron density level ( $N_p$ ), which would just cause cutoff of the doppler beam signal. The doppler beam is generated at a frequency of 13.3 GHz. Therefore, equating the beam frequency to the plasma frequency,

$$\omega = 2\pi \times 13.3 \times 10^9 = \omega_p = \left( \frac{N_p e^2}{\epsilon_0 m_e} \right)^{1/2}$$

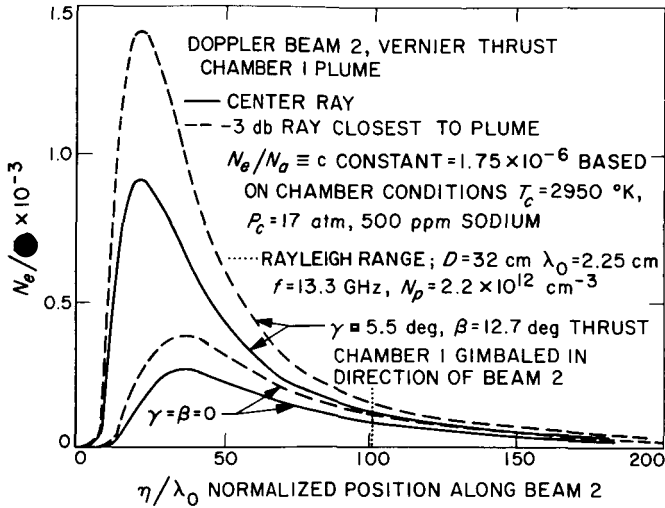
where  $e$  and  $m_e$  are the electronic charge and mass, respectively, and  $\epsilon_0$  is the permittivity of free space, we find that:  $N_p = 2.2 \times 10^{12} \text{ cm}^{-3}$ , and where  $N_p$  is the cutoff electron density.

Figure 5 is a plot of the normalized electron density  $N_e/N_p$  vs the distance along the antenna-ray axis  $\eta$  normalized to the freespace wave length  $\lambda_0 = 2.25$  cm. The four cases of concern are shown, i.e., the two rays and two gimbal angles of interest. As indicated previously, the bulk of the beam-plume intersection will occur within the near field of the antenna (inside the Rayleigh range,  $l$ ) by virtue of the fact that most of the electron density encountered along the ray path is concentrated well within this range.

### C. Electron Collision Frequency, $\nu_e$

The attenuation of an electromagnetic wave propagating through a plasma (Ref. 3) is dependent on the degree of damping the individual electrons undergo when forced

<sup>2</sup>The results of these tests were communicated by H. Schuman of Hughes Aircraft Co. H. Schuman assisted Dr. Balwanz in conducting these tests at NRL. The results, as yet, have not been formally documented.

Fig. 5.  $N_e/N_p$  vs  $\eta/\lambda_0$ 

into oscillation by the electric field of the wave. At the low ionization levels encountered in the plume these collisions will, almost exclusively, be with neutral atoms. The averaged electron momentum exchange collision rate is:

$$v_c = N_a v_e Q_{ea}$$

where  $v_e$  is the electron mean thermal velocity and  $Q_{ea}$  the average electron atom cross section for elastic momentum exchange. As we wish to be conservative, i.e., determine the maximum possible collision frequency and hence, attenuation, the chamber temperature  $T_e$  will be used to calculate  $v_e$  as opposed to the use of the exit temperature, which is perhaps more realistic. As the velocity

depends upon the square root of temperature, this distinction could lead to a factor of  $\sim 2$  increase in  $v_e$ . Perusal of published elastic electron-atom momentum exchange cross section data for gases, representative of the combustion products and the alkali metals, permitted a reasonable estimate of the maximum expected cross section  $Q_{ea}$  to be made. This value is  $Q_{ea} = 3 \times 10^{-15} \text{ cm}^2$ . Now for  $T_e = 2950^\circ \text{K}$ ,  $v_e \simeq 3 \times 10^7 \text{ cm/sec}$ ;

$$v_c = 9 \times 10^{-8} N_a$$

As we have in Fig. 5 a plot of the normalized electron density along the various rays of interest, it is expeditious to relate collision frequency to  $N_e/N_p$  and additionally, to normalize the frequency by the beam frequency  $\omega$ .

$$N_e = c N_a \therefore N_a = \frac{N_e}{c} = \frac{N_e}{N_p} \left( \frac{N_p}{c} \right)$$

so:

$$\frac{v_c}{\omega} = 9 \times 10^{-8} \left( \frac{N_e}{N_p} \right) \frac{N_p}{c \omega} = 1.4 \left( \frac{N_e}{N_p} \right)$$

As seen from Fig. 5,

$$\frac{N_e}{N_p} < 2 \times 10^{-3} \therefore \frac{v_c}{\omega} < 3 \times 10^{-3}$$

therefore, the plasma only very weakly attenuates the beam.

## VI. BEAM-PLUME INTERACTION

### A. Relative Propagation Constant $K^*$

The propagation of a plane, plane-polarized monochromatic electromagnetic wave in an isotropic inhomogeneous plasma (inhomogeneous in the direction of propagation  $\eta$ ), can be described in terms of its electric ( $E$ ) field by the wave equation:

$$\frac{d^2 \tilde{E}}{d\eta^2} + k^{*2}(\eta) \tilde{E} = 0$$

where  $E = \tilde{E} e^{i\omega t}$ , and  $k^*(\eta)$  is the complex propagation constant. It is convenient to normalize  $k^*$  by the propagation constant for free space ( $k_o = 2\pi/\lambda_o$ ).

$$K^* = \frac{k^*}{k_o} = \frac{k_r}{k_o} - \frac{ik_i}{k_o} = K_r - iK_i$$

It can be shown that  $K^*$  (Ref. 4) is related to the macroscopic properties of the plasma, i.e.,  $N_e$  and  $v_e$  as follows:

$$K_r = \frac{1}{(2)^{1/2}} \left\{ (1 - P) + \left[ (1 - P)^2 + P^2 \left( \frac{v_e}{\omega} \right)^2 \right]^{1/2} \right\}^{1/2}$$

$$K_i = \frac{1}{(2)^{1/2}} \left\{ -(1 - P) + \left[ (1 - P)^2 + P^2 \left( \frac{v_e}{\omega} \right)^2 \right]^{1/2} \right\}^{1/2}$$

where

$$P = \frac{\frac{N_e}{N_p}}{1 + \left( \frac{v_e}{\omega} \right)^2}$$

For the present case  $N_e/N_p$  and  $v_e/\omega \ll 1$ , which permits us to write:

$$P \simeq \frac{N_e}{N_p}$$

and

$$K_r \simeq 1 - \frac{N_e}{2}, \quad K_i \simeq \frac{1}{2} \left( \frac{N_e}{N_p} \right) \left( \frac{v_e}{\omega} \right)$$

where of course

$$\frac{N_e}{N_p} = \frac{N_e(\eta)}{N_p}$$

Note that we could write the imaginary part of the relative propagation constant  $K_i$  as  $0.7 (N_e/N_p)^2$  where we have assumed  $T_e$  and  $Q_{ae}$  (and  $c$ ) as being constant.

### B. Applicability of the Phase Integral (WKB) Method

Where gradients in the propagation constant are small, it is possible to use the phase integral approach, i.e., geometrical optics, to describe the propagation of a wave through an inhomogeneous media. In general, this technique requires that the electromagnetic wave be plane, i.e., the direction and amplitude are the same over distances, which are large in comparison to a wave length, and that the direction of propagation is normal to the wave surface. In essence, geometrical optics correspond to the limiting case of  $\lambda_o \rightarrow 0$ . The criteria that needs to be satisfied for the application of this approximation is:

$$\frac{\nabla \bar{K}^*}{K^*} \cdot \bar{\eta} < \frac{2\pi}{\lambda_o}$$

where  $\bar{\eta}$  is the unit vector in the direction of propagation.

Substitution of the expressions for  $K^*$  into the above relationship results in:

$$-\frac{\left[1 + i2.8 \frac{N_e}{N_p}\right]}{\left[2 - \frac{N_e}{N_p} - i1.4 \left(\frac{N_e}{N_p}\right)^2\right]} \frac{d\left(\frac{N_e}{N_p}\right)}{d\left(\frac{\eta}{\lambda_o}\right)} \simeq \frac{1}{2} \frac{d\left(\frac{N_e}{N_p}\right)}{d\left(\frac{\eta}{\lambda_o}\right)} < 2\pi$$

This criteria is easily satisfied even for the worst case of the  $-3$ -db ray,  $\gamma = 5\frac{1}{2}$  deg situation at the point of maximum slope ( $\eta/\lambda_o \simeq 10$ , cf Fig. 5). It should be pointed out that the near field region of an antenna is generally characterized by quite complex (non-planar) phase fronts. In addition, the wave is propagated through a three-dimensional electron density profile, and we have tacitly assumed that the plasma was uniform, transverse to the direction of propagation. While these two factors would tend to vitiate the use of geometrical optics, their precise influence is thought to be small. That is, uncertainties associated with the use of this technique are commensurate with those introduced by the previous assumptions.

The geometrical optical or phase integral technique permits one to describe the propagation of a wave in an inhomogeneous medium in terms of local conditions along the ray path

$$\tilde{E} = \tilde{E}_o \exp \left[ -ik_o \int_{\eta_o}^{\eta} K^* d\eta \right]$$

### C. Phase Shift

The phase  $\phi_p$  of the wave propagating through the plasma is dependent upon the real part of the propagation constant, i.e.,

$$\phi_p = k_o \int_{\eta_o}^{\eta} K_r d\eta = 2\pi \int_{\eta_o/\lambda_o}^{\eta/\lambda_o} K_r d\left(\frac{\eta}{\lambda_o}\right)$$

The phase change  $\Delta\phi$  is then the difference between the phase in plasma  $\phi_p$  and that calculated for free space conditions, i.e.,  $\phi_o = 2\pi\Delta(\eta/\lambda_o)$

Therefore,

$$\begin{aligned}\Delta\phi &= 2\pi \int_{\eta_o/\lambda_o}^{\eta/\lambda_o} \left( 1 - \frac{N_e(\eta)}{2N_p} \right) d\left(\frac{\eta}{\lambda_o}\right) - 2\pi\Delta \frac{\eta}{\lambda_o} \\ &= -\pi \int_{\eta_o/\lambda_o}^{\eta/\lambda_o} \frac{N_e(\eta)}{N_p} d\left(\frac{\eta}{\lambda_o}\right) \text{rad}\end{aligned}$$

for one-way propagation.

The two-way phase shift due to the presence of the plume and exclusive of phase shifts caused upon reflection from the surface is:

$$-2\pi \int_{\eta_o/\lambda_o}^{\eta/\lambda_o} \frac{N_e(\eta)}{N_p} d\left(\frac{\eta}{\lambda_o}\right) \text{rad}$$

The normalized electron density profiles of Fig. 5 were developed on the basis of maximum thrust (47 kgf) operation of the thrust chamber. To evaluate the effects of throttling upon the phase shift, it will be assumed that the combustion efficiency and flow characteristics of the nozzle are independent of thrust level. With these assumptions, then  $N_e/N_p$  would be directly proportional to the thrust level. Table 1 summarizes the calculated (by numerical integration of the  $N_e/N_p$  profiles) two-way phase shifts to be expected for the two ray paths, two gimbal positions and two thrust (T) levels (maximum = 45 kgf, minimum = 13.6 kgf).

**Table 1. Two-way phase shifts**

Condition	$\gamma = 0 \text{ deg}$		$\gamma = 5\frac{1}{2} \text{ deg}$	
	$T_{\max}$	$T_{\min}$	$T_{\max}$	$T_{\min}$
Central ray, deg	-7.3	-2.1	-16.3	-4.2
-3-db ray closest to plume, deg	-9.9	-2.8	-24.1	-7.1

The doppler velocity sensing system would be affected by variable phase shifts. Therefore, it is meaningful to present the data of Table 1 in a somewhat different format, which would emphasize the effects that gimbaling and throttling of the vernier thrust chamber would have on the two-way phase shift. To do this, we take as a nominal condition,  $\gamma = 0$ , and an average thrust level of 30.4 kgf. This corresponds to a phase shift of -4.7 deg for the central ray and -6.3 deg for the -3-db ray closest to the plume. These calculations are summarized in Table 2.

**Table 2. Change in two-way phase shift from normal**

Condition	$\gamma = 0 \text{ deg}$		$\gamma = 5\frac{1}{2} \text{ deg}$	
	$T_{\max}$	$T_{\min}$	$T_{\max}$	$T_{\min}$
Central ray, deg	-2.6	+2.6	-11.6	+0.5
-3-db ray closest to plume, deg	-3.6	+3.5	-17.8	-0.8



The preceding calculations were based on estimates of the maximum possible plume electron density levels. Analysis of the RADVS system suggests nonstatic phase-shifts less than one deg would not significantly influence overall system performance. The actual electron density levels and the phase shifts are probably lower than those shown in Table 2. However, the results indicate that the plume could interfere with the doppler velocity sensor system.

#### D. Attenuation

The attenuation of the beam is dependent upon the imaginary part of the relative propagation constant, i.e.,

$$\int_{\eta_0}^{\eta} \exp[-K_i(\eta)] d\eta = \int_{\eta_0/\lambda_0}^{\eta/\lambda_0} \exp\left[-\pi\left(\frac{N_e}{N_p}\right)\left(\frac{v_c}{\omega}\right)\right] d\left(\frac{\eta}{\lambda_0}\right)$$

or the attenuation of the electric ( $E$ ) field strength for one-way propagation of the wave is:

$$\int_{\eta_0/\lambda_0}^{\eta/\lambda_0} \exp\left[-1.4\pi\left(\frac{N_e}{N_p}\right)^2\right] d\left(\frac{\eta}{\lambda_0}\right)$$

Since the signal strength is proportional to  $E^2$  the overall attenuation of the signal because of two-way propagation through the plume, neglecting the losses associated with the reflection process is:

$$\int_{\eta_0/\lambda_0}^{\eta/\lambda_0} \exp\left[-5.6\pi\left(\frac{N_e}{N_p}\right)^2\right] d\left(\frac{\eta}{\lambda_0}\right)$$

In terms of db of attenuation, i.e.,

$$\text{db attenuation} = 10 \log_{10} \int_{\eta_0/\lambda_0}^{\eta/\lambda_0} \exp\left[-5.6\pi\left(\frac{N_e}{N_p}\right)^2\right] d\left(\frac{\eta}{\lambda_0}\right)$$

The results of the numerical integration of the above expression for the two rays and the two gimbal positions of interest are shown in Table 3 for the case of maximum thrust.

**Table 3. Two-way signal attenuation**

Condition	$\gamma = 0 \text{ deg}$	$\gamma = 5 \frac{1}{2} \text{ deg}$
Central ray, db	$-3.2 \times 10^{-4}$	$-1.7 \times 10^{-3}$
-3-db ray closest to plume, db	$-4.9 \times 10^{-4}$	$-4.0 \times 10^{-3}$

No attempt was made to determine the attenuation associated with the less severe minimum thrust case. In all cases the indicated attenuation is well below 0.1 db, a value at which attenuation effects begin to noticeably affect the performance of the RADVS system.

### E. Reflections from the Plume

Application of the phase integral method to the problem of reflections from arbitrary electron density profiles shows that in the first approximation there is no reflection. However, the following expression for the reflection coefficient  $\mathcal{R}$  (i.e., the ratio reflected to incident  $E$  fields) is obtained (Ref. 3) using the second order terms of the series

$$\mathcal{R} \equiv \frac{E_{\text{ref}}}{E_{\text{inc}}} \simeq \left\{ -\exp\left(2ik_o \int_{\eta_o}^{\eta} K^* d\eta\right) \right\} \left\{ \int_{\eta_o}^{\infty} \frac{\left(\frac{dK^*}{d\eta}\right)}{2K^*} \left[ \exp\left(-2ik_o \int_{\eta_o}^{\eta} K^* d\eta\right) \right] d\eta \right\}$$

To facilitate computation, the small amount of damping represented by the imaginary part of  $K^*$ , i.e.,  $K_i$ , will be neglected. This permits us to write:

$$\mathcal{R} \simeq \left\{ \exp\left[4\pi i \int_o^{\eta/\lambda_o} \left(1 - \frac{N_e}{N_p}\right) d\left(\frac{\eta}{\lambda_o}\right)\right] \right\} \left\{ \int_o^{\infty} -\left(\frac{d\left(\frac{N_e}{N_p}\right)}{d\left(\frac{\eta}{\lambda_o}\right)}\right) \left\langle \frac{\exp\left[-4\pi i \int_o^{\eta/\lambda_o} \left(1 - \frac{N_e}{N_p}\right) d\left(\frac{\eta}{\lambda_o}\right)\right]}{4} \right\rangle d\left(\frac{\eta}{\lambda_o}\right) \right\}$$

having set  $\eta_o/\lambda_o$  equal to zero. Because of the involved nature of this expression, only one case was numerically evaluated: the  $\gamma = 5\frac{1}{2}$  deg,  $-3$ -db ray case. The quantity of ultimate interest is the reflection coefficient for the signal, defined as  $\mathcal{R}\mathcal{R}^*$ , where  $\mathcal{R}^*$  is the complex conjugate of  $\mathcal{R}$ . The results of the numerical evaluation of this quantity indicate that the reflected energy would be a factor of  $\sim 2.2 \times 10^{-11}$  of the transmitted energy. In terms of db then, the reflected energy is  $\sim -106$  db below the transmitted signal. As the operation of the RADVS system would not be affected by the signals reflected from the plume which are  $-90$  db, or more, below the level of the transmitted signal, the presence of the plume would not impair the proper operation of the system.

### F. Bending of the Beam

The radius of curvature ( $R_c$ ) of the beam ray can be shown (Ref. 4) to be represented by the expression:

$$R_c \geq \frac{2\lambda_o \left(1 - \frac{N_e}{N_p}\right)}{\frac{d\left(\frac{N_e}{N_p}\right)}{d\left(\frac{\eta}{\lambda_o}\right)}}$$

However, implicit in our use of a basically one dimensional model of the plume, as discussed above, is the assumption that the plume is uniform in a direction normal to the ray (direction of propagation). It can be rigorously demonstrated (Ref. 4) that no matter how involved the variation of the propagation constant is in a region bounded by two planes  $\eta = 0$ ,  $A$  ( $0 \leq \eta \leq A$ ), the change in ray direction will be determined by the propagation constants to the left of  $\eta = 0$  and to the right of  $\eta = A$ , provided  $N_e < N_p$ . In our case, the region close to the antenna ( $\eta \leq 0$ ) and

far from the plume ( $\eta \leq A$ ) are regions characterized by the vacuum propagation constant,  $k_o$ . Therefore, use of the simple (one dimensional) model leads to the conclusion that there will be no bending of the ray. However, since it was not possible in the time allocated to this study to calculate the effects of the three dimensionality of the electron density profile, it was necessary to try and make an estimate of the maximum possible curvature the beam could undergo. This was done by assuming that the maximum gradient in electron density (occurring for the case of  $\gamma = 5\frac{1}{2}$  deg, -3-db ray, at  $\eta/\lambda_o \simeq 10$  (Fig. 5) extended over an arbitrarily large region of some  $50 \lambda_o$ , and by neglecting the compensating negative gradients. This calculation showed that at most, the curvature could be  $3 \times 10^{-3}$  rad, which is compared with the threshold value at which this effect first starts to influence RADVS system performance. This leads one to conclude that the beam will not be significantly bent by the presence of the plume. The assumption applied earlier of straight beam rays, is seen to be justified.

There is one influence of the one-dimensional (plane stratified) plume model that requires comment; namely, that while this model precludes bending of the beam by the electron density gradients (the rays enter and leave the plume at the same angle as long as  $N_e < N_p$ , the entering and exiting rays will suffer lateral displacement. It is straight forward to show that this displacement ( $\delta$ ) is, to an adequate level of approximation, represented by the expression

$$\delta \simeq \lambda_o \int_0^{\eta/\lambda_o} \left( \frac{N_e}{N_p} \right) d\left( \frac{\eta}{\lambda_o} \right)$$

Again, considering the worst case (-3-db ray,  $\gamma = 5\frac{1}{2}$  deg) evaluation of this expression shows that the displacement will be less than 2mm, a completely negligible amount.

Consequently, there should be no significant bending or displacement of the beam caused by the presence of the plume.

## VII. SUMMARY AND CONCLUSIONS

The *Surveyor* RADVS system was analyzed to determine if there would be significant interaction between the electrons in the vernier thrust chamber exhaust plume and the altimeter and doppler beams. Specifically, the worst case of interaction, i.e., between doppler beam No. 2 and vernier thrust chamber plume No. 1, was investigated in detail. It was assumed that the maximum specification propellant impurity level (500 ppm) was composed solely of sodium. This permitted the thrust chamber ionization level to be determined. Frozen flow conditions were then assumed to prevail, permitting the electron density profile of the exhaust plume to be calculated. It should be appreciated that these assumptions exaggerate the electron density level as the propellant impurity concentration is probably on the order of 10 ppm and recombination undoubtedly occurs, to a certain extent, in the nozzle and the plume (although, for the assumed sodium concentration, good correlation was obtained between theoretical and experimentally determined exhaust plane electron density levels). Application of the phase integral technique (geometrical optics) permitted the interaction between the doppler beam and the electrons in the plume to be evaluated. The results of this evaluation are summarized in the following paragraphs.

### A. Phase Shift

There is a possibility that two-way (i.e., the transmitted beam and the returning beam, neglecting effects attributable to the characteristics of the surface) nonstatic phase shifts of up to 18 deg could occur for various levels of thrust chamber gimbal angle and throttling level. The threshold value for phase-shift, above which the RADVS-system operation would be affected, is  $\sim 1$  deg. However, it should be reemphasized that these calculations were performed on the basis of the maximum allowable propellant impurity level (500 ppm) being pure sodium. Since the phase shift ( $\phi_p$ ) is directly proportional to the ionization level  $c$ , any reduction in the contamination level would be reflected as a decrease in  $c$  and a proportional diminution of  $\phi_p$ .

### B. Attenuation

The maximum calculated two-way attenuation is less than  $10^{-2}$  db which is well below the allowed 0.1 db.

### C. Reflection

The operation of the RADVS system would not be impaired provided that the signal reflected from the plume is at least 90 db below the transmitted signal level. Under the worst condition of gimbal angle, beam-ray position and thrust level, the maximum calculated reflection level is 106 db below the transmitted level.

### D. Beam Bending and Displacement

Under the most exaggerated conditions the calculated bending of the beam will be approximately equal to the threshold value of 2 mrad, above which the operation of the RADVS system would be influenced. The beam would be laterally displaced an amount computed to be less than 2 mm, due to its passage through the plume.

Therefore, it is concluded that, under the most severe conditions of geometry and thrust chamber operating levels, the phase shift associated with the two-way passage of the doppler beam could be of sufficient magnitude to influence the operation of the RADVS system. The two-way beam attenuation, bending, displacement and the back scattering from the plume were found not to influence the RADVS system, under the most severe operating conditions.

It should be pointed out that two factors were not considered in this analysis; turbulence in the plume and the presence of dust particles caused by impingement of the plume on the lunar surface. Turbulence could lead to a nonsteady increase in the reflectivity of the plume, and the presence of dust could lead to an increase in the electron density level. Moreover, the analysis is based on a one-dimension geometrical-optic treatment of the beam-plume interaction, three dimensional effects having been neglected. The magnitude of these effects is thought to be comparatively small, but they should be evaluated as part of any future study.

## REFERENCES

1. Surveyor Spacecraft, A-21 Model Description, Report 22484713, Hughes Aircraft Company, Culver City, Calif., March 1, 1965.
2. Molmud, P., *Estimates of Interference Due to Vernier Exhaust to be Encountered by Radar and Altimeter Systems During Lunar Landing*, Part II, Report 2586-62, Part II, Space Technology Laboratory, Redondo Beach, Calif.
3. Ginzburg, V. L., *Propagation of Electromagnetic Waves in Plasma*, Gordon and Breach, New York, 1960.
4. Kelso, J. M., *Radio Ray Propagation in the Ionosphere*, McGraw-Hill Book Company, Inc., New York, 1964.